Mass Flow Rate Measurement of Pneumatically Conveyed Solids Through Multi-modal Sensing and Data Driven Modelling

Faisal Abbas, Yong Yan, *Fellow, IEEE*, and Lijuan Wang, *Senior Member, IEEE*

***Abstract*—Online continuous measurement of mass flow rate of pneumatically conveyed solids is desirable in the monitoring and optimization of a range of industrial processes such as food processing, chemical engineering and power generation. This paper introduces a technique for the mass flow rate measurement of pneumatically conveyed solids based on multi-modal sensing and data driven modelling. The multi-modal sensing system is comprised of an array of ring-shaped electrostatic sensors, four arrays of arc-shaped electrostatic sensors and a differential-pressure transducer. Data driven models, including artificial neural network (ANN), support vector machine (SVM), and convolutional neural network (CNN), are established through training with statistical features extracted from the post-processed data from the sensing system. Statistical features are shortlisted based on their importance by calculating the partial mutual information between the features and the corresponding reference mass flow rate of solids. Experimental work was conducted on a laboratory-scale rig to train and test the models on both horizontal and vertical pipelines with particle velocity ranging from 10.1 m/s to 36.0 m/s and mass flow rate of solids from 3.2 g/s to 35.8 g/s. Experimental results suggest that the ANN, SVM and CNN models predict the mass flow rate of solids with a relative error within ±18%, ±14% and ±8%, respectively, under all test conditions. The predicted mass flow rate measurements with the ANN, SVM and CNN models are repeatable with a normalized standard deviation within 14%, 8% and 5%, respectively, under all test conditions.**

***Index Terms*–** Gas-solid flow; mass flow rate of solids; multi-modal sensors; artificial neural network; support vector machine; convolutional neural network.

I. Introduction

Bulk material is pneumatically conveyed in many industrial processes such as steel manufacturing, food processing, chemical engineering, cement production, and power generation. On-line continuous measurement of the mass flow rate of solids in pneumatic conveying pipelines is essential to balance the mass and energy and further to control energy efficiency and raw material consumption. The volumetric concentration of solids in a pneumatic conveying pipeline is often very dilute and commonly less than 0.1% by volume, which exhibits another renowned measurement challenge [1]. Based on the principle of measurement, all the techniques proposed in the literature can be divided into direct and indirect categories. A range of measurement techniques based on a variety of sensing principles, such as electrostatic [2], optical [3], acoustic [4], ultrasonic [5], capacitive [6] sensors and nuclear magnetic resonance [7] have been developed. All these types of sensor have the advantage of being non-intrusive and capable of measuring the mass flow rate of solids under certain process conditions. Amongst these techniques, the electrostatic sensors coupled with correlation signal processing algorithms provide a promising practical solution to the measurement of particle velocity due to their advantages over other sensing techniques, such as robustness in a hostile environment, non-intrusiveness in operation, and inexpensive capital cost and low maintenance requirements [2, 8]. In addition, signals from electrostatic sensors are sensitive to moving solids with little influence of the physical properties of solids being accumulated in the pipe that adversely affect other sensing techniques [9]. The conventional method for mass flow rate measurement of solids through electrostatic sensing is inferential, i.e. the mass flow rate of solids is derived from the measured particle velocity and concentration of solids, while the latter is measured through root mean square (RMS) level of the electrostatic sensor output [10, 11]. This inferential method of measuring the mass flow rate of solids is widely deployed [11, 12]. However, despite the advantages of electrostatic sensors for particle velocity measurement, the main problem in applying such a sensing technique is to relate the solids concentration to the RMS level of the sensor output, which depends on various physical factors, including particle velocity, ambient conditions, pipe orientations and solids size/shape etc [2]. It is worth noting that different particle velocities affect the measurement of solids concentration and hence the mass flow rate of solids in the inferential method [13].

With the advent of data driven techniques in the field of instrumentation and measurement, it is worth exploring data driven modelling as a potential method for mass flow rate measurement of solids with a minimized impact of the particle velocity, pipe orientation and inhomogeneous distribution of solids across the pipe cross section [2]. In view of the difficult and dynamic behaviour of solids in a pneumatic pipeline, multi-channel electrostatic sensor arrays are proposed to overcome the limitations of a single sensor for the measurement of mass flow rate of solids [14]. The data driven models, in this case, also offer the methodical way of combining the data from multiple sensors. Over the past few years, data driven models have been applied to measure gas-liquid two-phase flow [15].

Faisal Abbas, Yong Yan, Lijuan Wang are with School of Engineering, University of Kent, Canterbury, CT2 7NT, U.K. (e-mail: y.yan@kent.ac.uk).

However, only a limited number of reports are found on gas-solid flow measurement using data driven models. There has been an earlier attempt to deploy data driven models to achieve the gas-solid flow measurement by establishing a relationship between characteristics of the sensors and the flow parameters. The authors of this paper proposed an initial method for mass flow rate measurement of solids through multi-modal sensing and the data driven models [16]. For a constant particle velocity 22.1 m/s, the support vector machine (SVM) model has given the best performance with a relative error within ±10%. Aminu et al. [17] proposed a neural network based technique coupled with an acoustic sensor to measure the mass flow rate and concentration of solids and the gas velocity in a gas-solid two-phase flow. The normalized root mean square error (NRMSE) for the prediction of mass flow rate of solids with the proposed methodology was 18%. Wang et al. [18] proposed a technique for the concentration measurement of coal/biomass/air three-phase flow through multi-sensor data fusion and adaptive neuro-fuzzy inference (ANFIS). It was found that the proposed ANFIS structure measures the concentration of pulverized coal and the biomass with a maximum error of 1.2% and 0.7%, respectively. Recently, Zhang et al. [19] proposed a technique based on an acoustic sensor and a feedforward neural network for the mass flow rate measurement of solids in a horizontal pneumatic conveying pipe. Adding the flow regime parameters, by extracting the fluctuation distribution index and circumferential fluctuation difference from the acoustic signal, in the model has reduced the average prediction error from 17.3% to 8.4% [19].

As the magnitude of signals from the electrostatic sensors depends on various physical factors, it is difficult to derive the concentration of solids from the outputs of the sensors. Despite of various studies over the past few years, there is still a lack of an effective system through electrostatic sensing for the mass flow rate measurement of solids under a wide range of conditions. Moreover, the suitability and performance of the SVM and deep learning algorithms such as convolutional neural network (CNN) for gas-solid two-phase flow measurement remain unknown. This paper presents a novel approach to mass flow rate measurement of solids through data driven modelling that is capable of compensating the effects of various flow conditions which adversely affect the inferential method for mass flow metering. Owing to the dependency of the magnitude of the signals from electrostatic sensors on particle velocity and other parameters, data driven models including artificial neural network (ANN), SVM and CNN may have the potential to reduce the error in the mass flow rate measurement of solids by mitigating the effects of various flow conditions. The data driven models are established through training and tested under a range of mass flow rates of solids, particle velocities and pipe orientations. The SVM model is also applied on the data of each sensor and different combinations of sensors to evaluate the importance of each sensor in terms of relative error in predicted mass flow rate measurements (see Section III-D). The experiments were conducted on a 50-mm bore pipe section on a laboratory-scale test rig. The performance of the proposed measurement system, in terms of accuracy and repeatability, is assessed under a range of test conditions.

II. Methodology

A. Overall Measurement Principle

The suggested solution to the measurement problem, as shown in Fig. 1, is based on multi-modal sensing and data driven models. The multi-modal sensing system includes an array of ring-shaped electrostatic sensors, four arrays of arc-shaped electrostatic sensors and a DP transducer. Electrostatic sensors are mainly chosen due to their high sensitivity to charged particles, non-intrusive characteristics, simple structure, and inexpensive capital cost [2]. The DP transducer can determine the drop in line pressure due to air-solids two-phase mixture flow in the pneumatic pipeline. After the signals from all the sensors are denoised, the statistical features are extracted from the data from all the electrostatic sensors and the DP transducer to train the data driven models. The required solids velocity, for the measurement of mass flow rate, is measured using all the ring and arc-shaped electrostatic sensors with data fusion and the correlation signal processing technique [11].

A data driven model is used to establish the complex relationship between the sensor data and the mass flow rate of solids to be measured. To determine the optimal number of inputs for the data driven models, extraction and selection of statistical features are undertaken prior to the development of the models. The optimal structures of the models are developed during the training and validation process. For the measurement of mass flow rate of solids, the data driven models are trained with the selected statistical features extracted from the post-processed sensor data in the time, frequency and the time-frequency domains. The raw sensor data is processed prior to the extraction of statistical features to avoid the false training with absurd data labels (see Section II-D). The proposed measurement strategy is implemented in the MATLAB version 2020b.

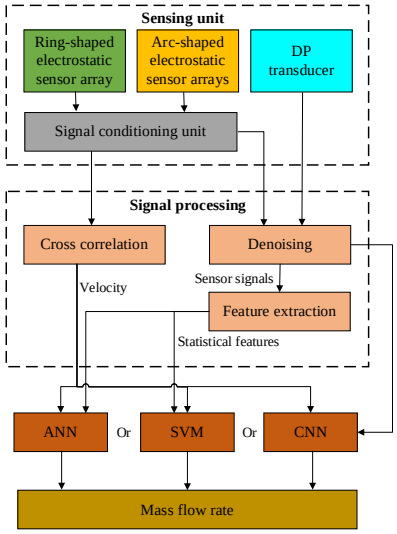

Fig. 1. Principle of mass flow rate measurement through modal sensing and data driven modelling.

B. Multi-modal Sensors

The simplified schematic of the sensing head, used in this study, is shown in Fig. 2. The schematic of the electrodes is based on the design proposed by Qian and Yan [14]. The array of ring-shaped electrostatic sensors includes 4 electrodes (E1 to E4) that gives the cross-sectionally averaged flow parameters, whereas each of the four arrays of arc-shaped electrostatic sensors (a, b, c, d) includes four electrodes (E5 to E8) that give the localized flow parameters in an inhomogeneous flow regime. The mounting of these electrodes inside the pipe wall is shown in Fig. 3. The four arcs (a, b, c, d) in the whole cross-section of the pipe are a good trade-off between the cost of signal conditioning and covering the top, front, back and bottom area of the pipe. Solids distribution and particle velocity across the pipe can be extremely inhomogeneous and irregular, respectively which can result in producing dramatically fluctuating and inaccurate measurements [2]. Such irregular flow pattern can also result in an ill-defined correlation peak in particle velocity measurement [2]. One means of alleviating this issue is to use multi-channel sensor arrays in the measurement system. The use of multi-channel ring and arc-shaped electrostatic sensors may result in a reliable measurement of flow parameters in case one of the sensors is faulty [11]. As the varying concentration of solids in a pneumatic pipeline may also cause a change in the line pressure, therefore a DP transducer is also incorporated in the sensing system with the pressure holes between the two ends of the sensing head.

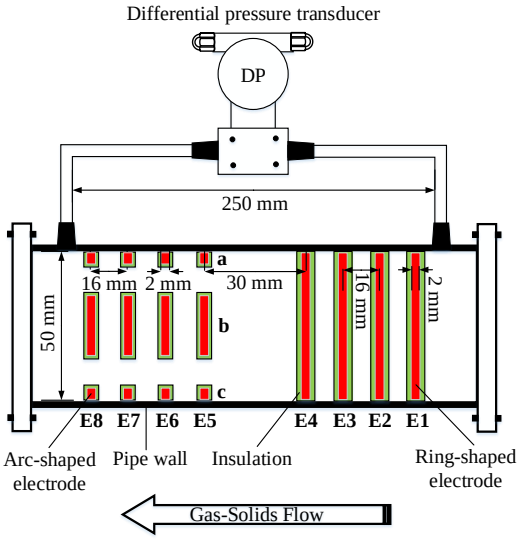

Fig. 2. Sensor arrangement in the sensing head.

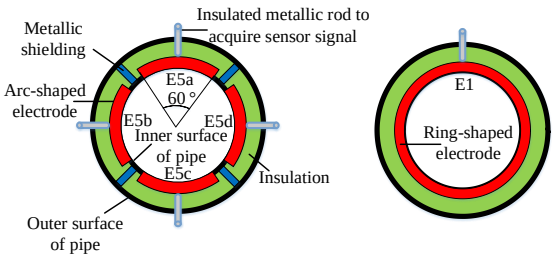

Fig. 3. Cross section of the electrostatic sensors.

C. Signal Conditioning

Fig. 4 shows a simplified block diagram of the signal conditioning elements and associated hardware. As the magnitude of the charge density on solids is as low as 10^{-7} C/kg [20], the weak current signal from an electrode is initially converted into a voltage signal via a pre-amplifier sitting right next to the electrode with a gain of 5 mV/nA. The bandwidth of the signals from the pre-amplifier is normally less than 1 kHz [21, 22]. The signal from the pre-amplifier is further amplified with a gain of 10 db and then passed to a second-order Sallen-Key low-pass filter with a cut-off frequency of 10 kHz to eliminate the high frequency noise that occurs mainly from external interferences [11]. A coupling capacitor is used to eliminate the DC component in the sensor signal. However, there may be minute DC residue in the final signal, so the remaining mean value is taken out in the pre-processing of the digitized signal. All the sensor signals are digitized using high-speed data acquisition (DAQ) card and then processed on the host computer. However, the DP transducer does not require any additional signal conditioning, so its signal is connected directly to the DAQ card.

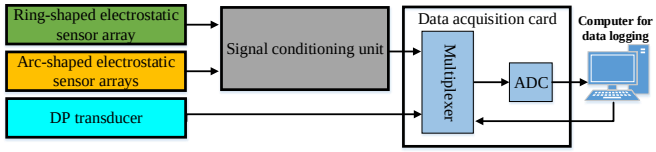

Fig. 4. Block diagram of the signal conditioning elements and associated hardware.

D. Feature Extraction

It is not straightforward to define the appropriate statistical features for the establishment and efficient training of data driven models (Section II-F) and the ultimate measurement of the mass flow rate of solids. An extensive literature review was carried out in this study to compile and consider all the possible statistical features that may be used as inputs for the data driven models. The magnitude of all the sensor signals varies with the movement of solids. Therefore, the data driven models are trained with statistical features based on the magnitude of each sensor signal in three different domains, including time, frequency, and time-frequency domains. Table I summarizes the symbols and the equations to extract the features from the outputs of the electrostatic sensors and the DP transducer. A total of 13 statistical features, including root mean square, mean, standard deviation, skewness, kurtosis, number of zero crossings, variance, peak to peak, entropy, simple sign integral, waveform length, Willison amplitude and slope sign integral, are extracted in the time domain. In the frequency domain five features, including peak amplitude, signal power, mean fluctuation frequency, spectral entropy and shape factor, are extracted. Likewise, mean, root mean square, variance, four quartile frequencies and mean crossing irregularity are also extracted in the time-frequency domain.

TABLE I
STATISTICAL FEATURES THAT ARE CONSIDERED IN THIS STUDY

	Description	Symbol	Equation

Time Domain	Root Mean Square	RMS_T	$\sqrt{\frac{1}{N}\sum_{i=1}^{N} x_i^2}$
	Mean	$\bar{x}$	$\frac{1}{N}\sum_{i=1}^{N} x_i$
	Standard Deviation	σ	$\sqrt{\frac{\sum_{i=1}^{N}\|x_i-\bar{x}\|^2}{N-1}}$
	Skewness	SKW	$\frac{1}{N\sigma^3}\left(\sum_{i=1}^{N}\|x_i-\bar{x}\|^3\right)$
	Kurtosis	KRT	$\frac{1}{N\sigma^4}\left(\sum_{i=1}^{N}\|x_i-\bar{x}\|^4\right)$
	Number of Zero Crossings	ZC	$(x_i > 0 \,\&\, x_{i+1} < 0) \,\|\|\, (x_i < 0 \,\&\, x_{i+1} > 0)$
	Variance	VAR_T	$\frac{1}{N-1}\left(\sum_{i=1}^{N}\|x_i-\bar{x}\|^2\right)$
	Peak to Peak	PP	Max(x)-Min(x)
	Entropy	H_T	$\sum_{i=1}^{N} p_i \log(p_i)$
	Simple Sign Integral	SSI	$\sum_{i=1}^{N}\|x_i\|^2$
	Waveform Length	WL	$\sum_{i=2}^{N}\|x_i - x_{i-1}\|$
	Willison Amplitude	WAMP	$\sum_{i=2}^{N} f(\|x_i - x_{i-1}\|)$
	Slope Sign Changes	SSL	$(x_i > x_{i-1} \,\&\, x_i > x_{i+1}) \,\|\|\, (x_i < x_{i-1} \,\&\, x_i < x_{i+1})$
Frequency Domain	Peak Amplitude	A_p	$max(\|S\|)$
	Signal Power	SP	$\sum_{i=1}^{N} S(\mathrm{i})$
	Mean Fluctuation Freq.	FF	$\frac{\sum_{i=1}^{N} S(i)X(\mathrm{i})}{\sum_{i=1}^{N} S(\mathrm{i})}$
	Spectral Entropy	SE	$-\sum_{i=1}^{M} d_i \log_{10}(d_i)$
	Shape Factor	SF	$\frac{1}{\bar{S}}\left(\sqrt{\frac{1}{N-1}\sum_{i=1}^{N}(S_i-\bar{S})^2}\right)$
Time-Frequency Domain	Mean	$\bar{C}$	$\frac{1}{N^2}\sum_{i=1}^{N}\sum_{j=1}^{N} C_{i,j}$
	Root Mean Square	RMS_{TF}	$\sqrt{\frac{1}{N^2}\sum_{i=1}^{N}\sum_{j=1}^{N} C_{i,j}^2}$
	Variance	VAR_{TF}	$\frac{1}{N-1}\left(\sum_{i=1}^{N}\sum_{j=1}^{N}\|C_{i,j}-\bar{C}\|\right)^2$
	Quartile Freq. 1	QFR1	f_{25}/f_{75}
	Quartile Freq. 2	QFR2	f_{25}/f_{90}
	Quartile Freq. 3	QFR3	f_{50}/f_{75}
	Quartile Freq. 4	QFR4	f_{50}/f_{90}
	Mean Crossing Irregularity	MCI	$\frac{1}{\bar{C}}\sqrt{VAR_{TF}}$

Where,

x = Samples of the sensor signal

N = Total number of samples

p = Probability distribution of x

f = Function to check if the difference is higher than pre-defined threshold

X = Discrete Fourier transform of x

d = Probability distribution of S

S = Power spectrum

$\bar{S}$ = Mean of power spectral density

C = Resultant of the continuous wavelet transform

$\bar{C}$ = Mean of the continuous wavelet transform

f_{25}, f_{50}, f_{75}, f_{90} = Frequency where the power of the signal reaches 25%, 50%, 75%, and 90% of the total power of the signal, respectively.

E. Feature Selection

There are total of 546 features extracted from 21 post-processed sensor signals. Some of the features are more important than others, while some may be intrinsically linked to each other or overlapped. The unnecessary and redundant features not only use extra memory storage but also raise over-fitting problems, wasting computing power, and all the time required for the purpose of training the models. With the use of the partial mutual information (PMI) algorithm [23], redundancy between some features, that look mathematically similar, can be identified. The PMI algorithm calculates only that information between input feature x and target output y which has not been accounted for the calculation of information between previously selected feature set w and output y. PMI for distinct data samples is represented as:

$$\mathrm{PMI} = \frac{1}{N}\sum_{i=1}^{N} log\frac{p(x',y')}{p(x')p(y')} \quad (1)$$

Where $x' = x - E[x/w]$ and $y' = y - E[y/w]$. Operator $E[\bullet]$ represents the expected value of the variable x or y, given variable w has already been selected. Note that $p(x')$, $p(y')$ and $p(x', y')$ are the respective univariate and joint probability densities estimated with a total of N samples. Therefore, if some features are already selected in w, then variables x' and y' are the residuals of a new feature x and the output y regarding the selected features in w, respectively.

Selecting a higher number of useful features can improve the performance of the data driven models. However, more features can also increase the complexity of the models. Therefore, the Akaike information criterion (AIC) is applied to identify the optimal number of features [24].

$$AIC = NLn\left(\frac{1}{N}\sum_{i=1}^{N} u_i^2\right) + 2p \quad (2)$$

where N is the number of samples, p is the number of model parameters and u is the residual of the desired output.

The procedure of selecting useful features is summarised as follows:

(1) Calculate the PMI value of all the features using Equation (1)

(2) Sort all the features in a descending order based on their PMI values

(3) Apply Equation (2) on all the features one by one, starting from the features with the highest PMI

(4) Keep selecting the features if the AIC decreases. Otherwise, terminate the selecting procedure.

It is worth noting that the feature selection is different from dimensionality reduction. Here the problem is not to reduce the

dimension but to remove the irrelevant and unwanted features while still having a sufficient number of features to keep the model's generalization intact. It should be noted that the feature selection is only implemented before the development of data driven models to determine the suitable inputs for data driven models. Once the most relevant features are determined, this step will no longer be required, and the models can be trained and tested with the short-listed features. The short-listed features are detailed in Section III-E.

F. Data Driven Models

Suitable data driven models are required to map the complex relationship between the sensor data and the mass flow rate of solids to be measured. In view of their advantages in multiphase flow measurement [25], as outlined in the Introduction section, three data driven models, including ANN, SVM, and CNN, are selected and deployed in this study. The architectures of the BP-ANN and SVM models are shown in Fig. 5 and Fig. 6, respectively. The input dimension of these models depends on the number of features selected in Section II-E. The number of neurons in the hidden layer is determined by [26]

$$L \leq 2M + 1 \tag{3}$$

$$L \leq \frac{N}{M+1} \tag{4}$$

where L is the number of neurons and N and M are the numbers of samples and features, respectively.

The ANN model is developed by training a network of neurons to represent the inherent relationship between the input data and the intended measurand on output. The ANN model, used in this research, is a three-layer feedforward network that is trained based on the backpropagation learning method. Nodes present in the hidden layer receive values from the input layer and passes a quantitative value on through a pre-defined activation function. An activation function in the ANN model performs the complex computation in the hidden layer and then transfers the outcome to the output layer. Activation functions are mainly used to introduce the non-linearity in the model [27].

SVM models are one of the most popular and widely implemented data driven algorithms which perform linear regression in a high dimensional feature space and tend to reduce model complexity. The type of SVM model, implemented in this research, is regression for the measurement of mass flow rate of solids. As the output is a real and continuous number, therefore it becomes very challenging to predict the information at hand which has infinite possibilities. In the case of regression, a margin of tolerance is set in approximation to the SVM which would have already requested from the problem. SVM regression is considered a non-parametric technique because it relies on kernel functions. The kernel trick is useful to minimize the computational complexity of the input data which is comprised of several statistical features in the original space.

The theory of artificial neural networks has given rise to the idea of deep learning. Unlike the neural networks that were developed many years ago, modern methods of deep learning have cracked the code for scale on big data, generalization, and training stability. These are the models powered by the information that can reach the best statistical accuracy when exposed to a high volume of data. Despite all the benefits that modern deep learning models have on traditional models, it is not guaranteed that deep learning models will always give an output of the best accuracy. There are many types of deep learning models available. As shown in

Fig. 7, the CNN model is the one implemented primarily in this research due to its simplicity and inexpensive cost of computing, compared to other deep learning models [28]. CNN is a deep learning class that is most widely used for image data processing and evaluation. The CNN model is able to interpret the information lying in the data from multiple sensors and suppress the redundancy through deriving the layer structures. The CNN model, therefore, accepts the direct post-processed sensor signals as inputs. The complexity and size of the layers in the CNN system are the key factors that must be addressed in the design of a CNN architecture. Including a larger number of convolution layers may help improve design quality by improving the consistency of the derived elements. However, at the same time, it can also increase the cost of processing and generate over-fitting issues. Therefore, it is a common practice to begin this layer design process with a very shallow model and then gradually add additional layers of different window sizes and stride values until the test accuracy reaches saturation (see Section III-E).

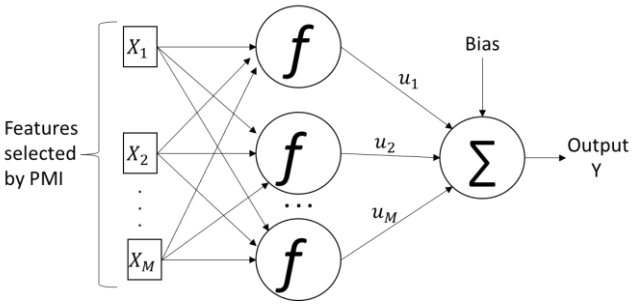

Fig. 5. Structure of ANN.

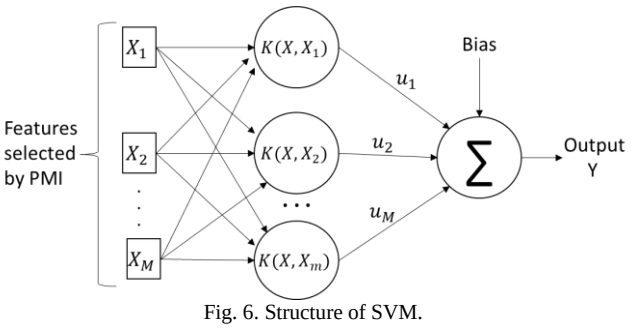

Fig. 6. Structure of SVM.

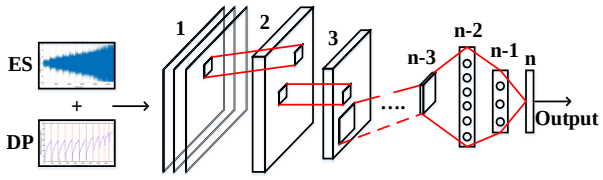

Fig. 7. Structure of CNN.

III. Experimental Results and Discussion

A. Experimental Setup and Test Conditions

As shown in Fig. 8 and Fig. 9, the experimental work detailed in this paper was conducted on a laboratory scale test rig. Concerning the health and safety reasons, experiments were conducted using flour particles that are mostly in round shape with the mean equivalent diameter of 0.21 mm measured with particle imaging system. The test rig is constructed with stainless steel pipes for abrasive resistance and is grounded for safety reasons. The sensing head, as discussed in Section II.B, is installed, respectively, on the horizontal pneumatic pipeline at a distance of 240 cm downstream of the particle and air inlet and in the middle of the vertical pipeline. Solids are placed on the upper surface of the vibratory feeder and are positioned and pointed towards the pipe inlet. The solids concentration and the air velocity are adjusted by regulating the intensity of vibrations of the feeder and the power of the suction pump using two independent variable frequency drives (VFD). A DAQ card is used to collect the sensor data from the signal conditioning circuit as shown in Fig. 4. After obtaining a request of variable frequency from the PC, a voltage signal is provided by the DAQ card to regulate the output frequency of the VFD.

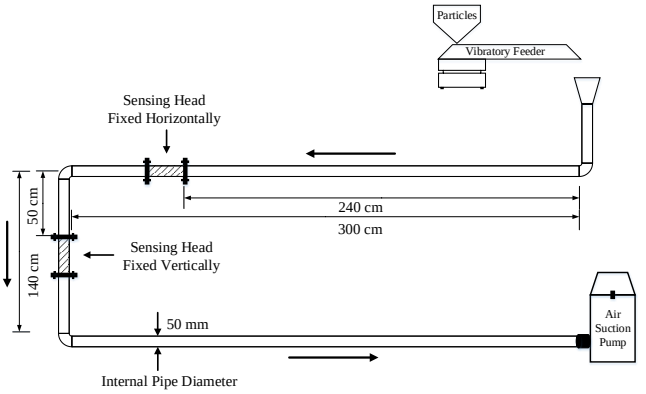

Fig. 8. Schematic of pneumatic rig.

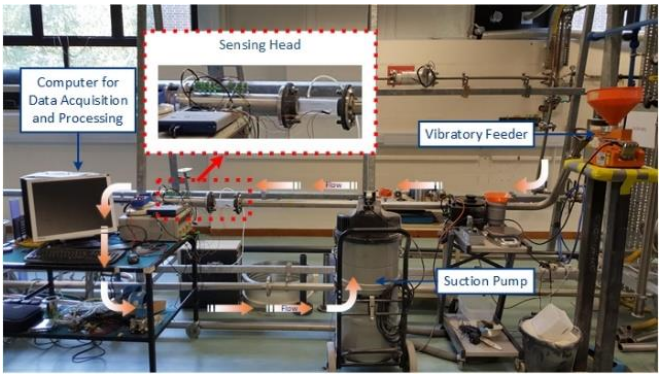

Fig. 9. Laboratory scale pneumatic rig.

In order to train and test the data driven models, a range of experiments were carried out to collect the data under horizontal and vertical pipe orientations while maintaining an average ambient temperature of 19 ℃ and average relative humidity of 54% with two commercial level air conditioning units. All the signals from the electrostatic sensors were sampled at 20 kHz whereas the output from the DP transducer was sampled at 1 kHz owing to the operating bandwidths of the sensors.

During the experimental work, data were collected with 11 mass flow rates of solids varying from 3.2 g/s to 35.8 g/s with an uncertainty of ±3% that is calculated based on ten measurements from each mass flow rate condition of solids. A weighing scale and a timer is used to determine the reference mass flow rates of solids. Data for each mass flow rate of solids were also recorded with 9 different air velocity conditions varying from 10.1 m/s to 36.0 m/s with an uncertainty of ±1%, calculated using ten samples of each air velocity measured with hot wire anemometer. For each combination of air velocity and mass flow rate of solids, the data is collected for 30 seconds. Fig. 10 shows the data points used for training and test conditions. It should be stressed that the data to test the models are classified into seen and unseen conditions. The seen test conditions include mass flow rates of solids which are also used for the training of models as listed in Table II. All the data in Table II is divided into 70% for training and 30% for testing. However, the unseen test conditions are kept entirely different from the mass flow rates of solids used for the training of models as listed in Table III. All the unseen test conditions are chosen in a way to assess the prediction accuracy of the data driven models for the points lying between two adjacent training points. Two of the unseen mass flow rate conditions, 3.2 g/s and 35.8 g/s, are chosen from outside the training and test data limits to evaluate the generalization ability of the models. The large gap of values between the higher mass flow rates of solids in the training data is due to nonlinear relationship between the VFD control and the mass flow rate of solids. The data driven models are made generalized enough to predict any value lying between two heavily spaced training conditions.

As the velocity and mass flow rate of solids is controlled, respectively, with the suction pump and the vibratory feeder through the VFD, the set points for velocity and mass flow rate are chosen based on the distribution of frequency values of the VFD. For example, a suitable range of VFD frequencies to control the vibratory feeder lies between 30 and 50 Hz. Therefore, eleven set points are chosen for mass flow rate by varying the frequency between 30 and 50 Hz with a difference of 2 Hz in every set point. It is worth noting that the relationship between the VFD frequency and the mass flow rates is not linear and hence this is the reason of having larger gaps at higher mass flow rates.

It should be noted that at lower air velocity conditions, higher mass flow rates are not workable because the particles will not be in a suspension in the pipeline, which may lead to blockage of the pipeline. The practically inappropriate combinations of a lower particle velocity and a higher mass flow rate of solids are marked out with a dash in Table II and Table III.

The flow pattern in the pipe varies with the mass flow rate and velocity of solids and other properties and this can go from a fully suspended flow (uniform mix of gas and solids phases) to highly stratified flow (larger particles move along the bottom of the pipe). However, seen and unseen conditions are mixed in

between each other, as shown in Tables II and III. Therefore, the flow pattern will remain more or less the same for both seen and unseen test conditions for a given narrow range of mass flow rate and velocity of solids. However, a noticeable difference in flow pattern was observed for the unseen test conditions at the two extreme ends of the range, i.e. 3.2 g/s and 35.8 g/s (Table III). These unseen conditions are created to evaluate the generalization capability of the models.

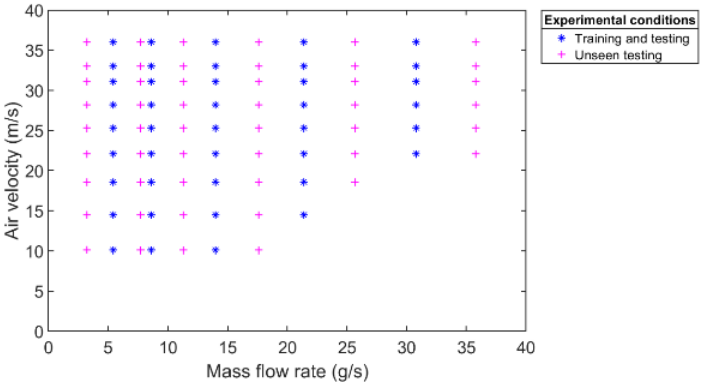

Fig. 10. Training and test conditions.

TABLE II
COMBINATIONS OF AIR VELOCITY AND MASS FLOW RATE FOR TRAINING AND TESTING OF MODELS

		Mass flow rate (g/s)				
		5.4	8.6	14.0	21.4	30.8
Air velocity (m/s)	10.1	✓	✓	✓	–	–
	14.5	✓	✓	✓	✓	–
	18.6	✓	✓	✓	✓	–
	22.1	✓	✓	✓	✓	✓
	25.3	✓	✓	✓	✓	✓
	28.2	✓	✓	✓	✓	✓
	31.1	✓	✓	✓	✓	✓
	33.0	✓	✓	✓	✓	✓
	36.0	✓	✓	✓	✓	✓

TABLE III
COMBINATIONS OF AIR VELOCITY AND MASS FLOW RATE FOR TESTING OF MODELS WITH UNSEEN CONDITIONS

		Mass flow rate (g/s)					
		3.2	7.7	11.3	17.6	25.7	35.8
Air velocity (m/s)	10.1	✓	✓	✓	✓	–	–
	14.5	✓	✓	✓	✓	–	–
	18.6	✓	✓	✓	✓	✓	–
	22.1	✓	✓	✓	✓	✓	✓
	25.3	✓	✓	✓	✓	✓	✓
	28.2	✓	✓	✓	✓	✓	✓
	31.1	✓	✓	✓	✓	✓	✓
	33.0	✓	✓	✓	✓	✓	✓
	36.0	✓	✓	✓	✓	✓	✓

B. Sensor Data Under Horizontal Pipe Orientation

Fig. 11 shows the post-processed signals under all the conditions from the ring-shaped electrostatic sensor (E1). All the boundaries, highlighted with red vertical lines, represent the sensor data under seen and unseen mass flow rates of solids, as listed in Table II and Table III, increasing from left to right. Sensor data plotted under the same mass flow rate condition also belong to the different air velocities, increasing from left to right. As can be seen, the amplitude of the signals increases with the mass flow rate as well as particle velocity. The signal conditioning unit is powered from a ±3.3 V power supply, therefore the magnitude of all the signals remains within ±3.3 V without saturation. Meanwhile, the signal conditioning unit is designed such that the range of the signals under all unseen test conditions is not out of the limits of the supply voltage ±3.3 V. The signals from other sensors are similar in terms signal patterns and ranges as all the signal conditioning units are powered from the same ±3.3 V power supply.

Fig. 12 shows the relationship between the RMS of a post-processed signal from the E1 electrode of the ring-shaped electrostatic sensor and the mass flow rate of solids under different air velocities. Each data point on the graph also indicates the uncertainty in both mass flow rate and RMS of electrostatic signal that is calculated from the reference data of mass flow rate of solids and the recorded electrostatic signal under different conditions. The magnitude of electrostatic signal increases nonlinearly by increasing the mass flow rate and the velocity of solids. Since a high volume of large solids (less surface charge) is concentrated at the bottom of the pipe due to gravitational effect, the RMS of the signal, obtained from the arc-shaped electrode at the bottom of the pipe, is lower than others, as shown in Fig. 13. Nevertheless, the RMS values from the electrodes at the front and back are comparatively higher than that at the bottom owing to the higher number of small particles in the suspension. The RMS of the signal from the sensor at the top is lower than those at the front and the back due to the lower solids concentration along the top of the pipe. However, at much lower mass flow rates (<10 g/s), the outputs from the top, front and the back electrodes yield very similar RMS magnitudes due to the fully suspended flow pattern except some large particles moving relatively slow at the bottom giving rise to a lower RMS. Fig. 14 shows the dependency of the differential pressure on the mass flow rate and velocity of solids in the pipeline. Drop in line pressure also increases nonlinearly with the mass flow rate of solids and air velocity due to higher friction faced by the solids with the pipe wall. The DP signal at lowest velocity is much lower than the signals at other velocity because the impact of air velocity 10.1 m/s is relatively lower on the line pressure. Each data point on the plot also shows the uncertainty calculated for reference data of mass flow rate of solids and the measured line pressure with the DP transducer.

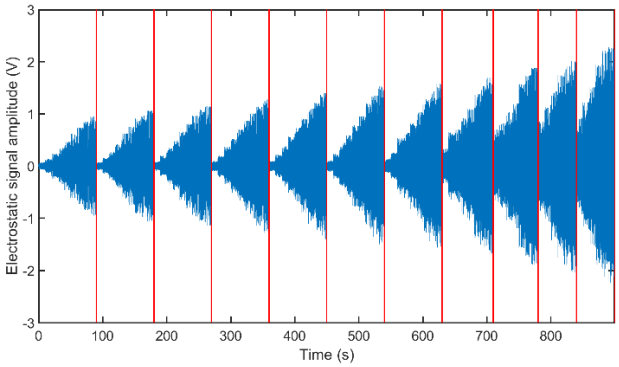

Fig. 11. Post-processed signals from the electrostatic sensor E1.

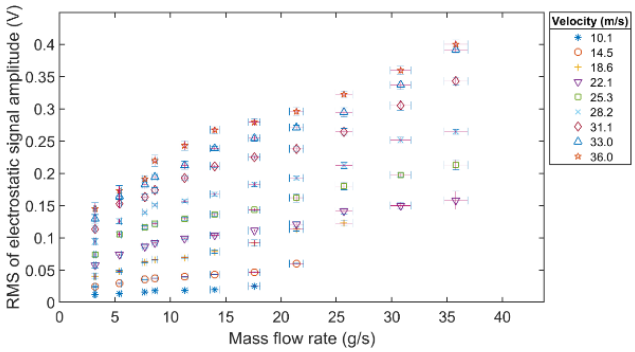

Fig. 12. RMS of the electrostatic signal from ring-shaped electrostatic sensor E1 under horizontal pipe orientation.

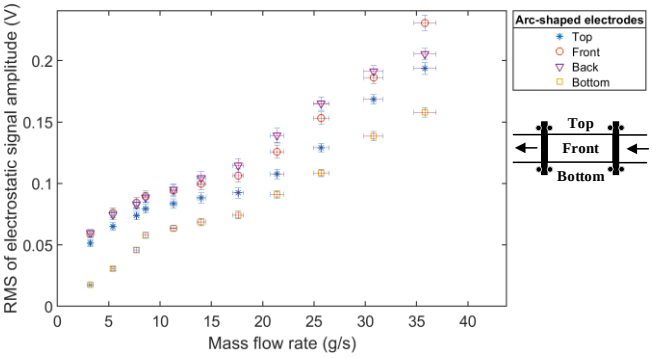

Fig. 13. RMS of electrostatic signal from arc-shaped electrostatic sensors E5a, E5b, E5c, E5d with air velocity 22.1 m/s under horizontal pipe orientation.

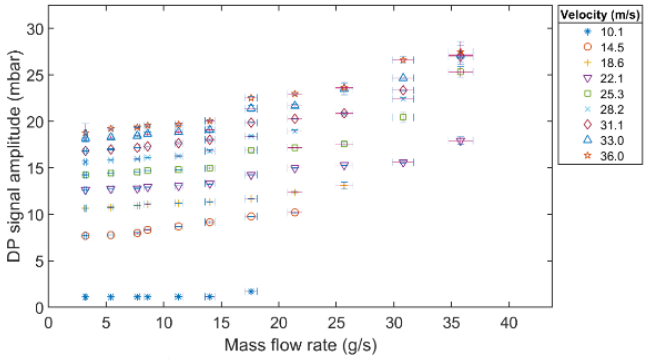

Fig. 14: Output of the DP transducer under horizontal pipe orientation.

C. *Sensor Data Under Vertical Pipe Orientation*

For each pair of air velocity and mass flow rate of solids, the magnitude of the signals from ring-shaped sensors in vertical pipe orientation is slightly increased compared to the horizontal pipe orientation due to higher gravitational effect and solids-pipe wall friction as shown in Fig. 15. However, a substantial variation is observed in the localized charge values due to change in flow regime under vertical pipe orientation, as shown in Fig. 16. The larger solids with less surface charge, moving along the upper horizontal pipeline, hit with the wall of the pipe bend and start moving along the left side of the vertical pipeline, resulting in lower RMS charge. The smaller, but more solids at the front, back and the right regions of the pipe yield higher RMS values for the signals from the sensors at such locations. Meanwhile, after downwards turning at the bend, fine particles at the right of the pipe give the lowest RMS value. The variations in the DP signal amplitude with the mass flow rate of solids under vertical pipe orientation is demonstrated in Fig. 17. The drop in the line pressure in this case is escalated a little compared to that in horizontal pipe orientation due to higher effect of gravity on the gas, solids, and the solids-wall friction at the pipe bend.

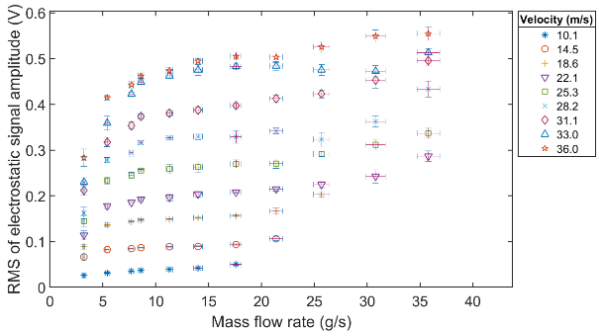

Fig. 15 RMS of the electrostatic signal from ring-shaped electrostatic sensor E1 under vertical pipe orientation.

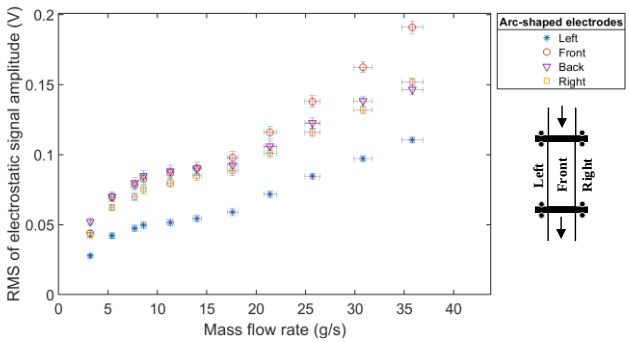

Fig. 16 RMS of electrostatic signal from arc-shaped electrostatic sensors E5a, E5b, E5c, E5d with air velocity 22.1 m/s under vertical pipe orientation.

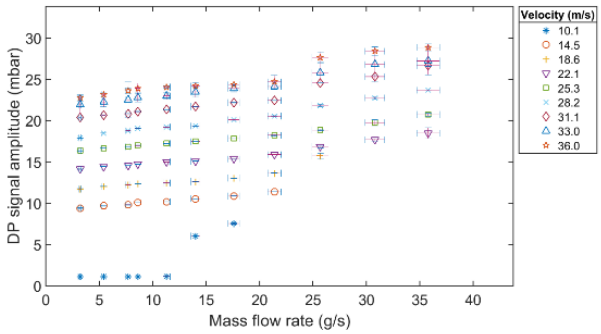

Fig. 17 Output of the DP transducer under vertical pipe orientation.

D. *Selection of Useful Sensors*

The usefulness of a sensor can be investigated through a model based selection method. The model is in a fixed structure with the same feature extraction mechanism. In this case, the sensor signal is the only factor affecting the performance of the model. As the SVM model has fixed three-layer structure and it takes a moderate volume of dataset and thus less time for training, therefore SVM model is applied to evaluate the importance of ring and arc-shaped electrostatic sensors and the DP transducer in this study. Three most commonly used features, including RMS, standard deviation and variance, are

extracted from the post-processed sensor signal as inputs to the SVM model. The model output is mass flow rate of solids. NRMSE is applied to assess the performance of the SVM models and it is determined from

$$NRMSE = \frac{1}{\bar{y}}\sqrt{\frac{1}{N}\sum_{k=1}^{N}(y_k - \widehat{y_k})^2} \quad (5)$$

where y_k (k = 1 to N) is the reference mass flow rate of solids, $\bar{y}$ is the mean of the mass flow rate of y_k, $\widehat{y_k}$ is the predicted solids mass flow rate and N is the total number of samples used. The sensor selection procedure is summarised as follows:

(1) Initialise the selected sensor set S with null, potential sensor set P with E1, E2, E3, E4, E5, E6, E7, E8, DP.
(2) Develop the SVM model based on each sensor from P combined with all the sensors in S.
(3) Find out the sensor which makes the model developed in step (2) yielding lowest NRMSE
(4) Move the sensor from P to S
(5) Repeat step (2) until P is empty

A total of 9 combinations will be obtained from (4) and the best combination is the determined by the lowest NRMSE or the NRMSE has reached a certain level.

The training and test data for the purpose of sensor selection come from the experimental data collected under horizontal pipe orientation, with a fixed air velocity of 22.1 m/s and all the mass flow rates described in Fig. 10. Fig. 18 shows the performance of SVM models which were developed based on the signals from each sensor respectively. The error bars indicate the standard deviation of errors in predicted mass flow rates of solids [25]. Since each set of arc-shaped electrodes is made up of top, front, back and the bottom arcs, it provides localized and yet more precise information about the whole cross-section of pipe. Therefore, NRMSE calculated with arc-shaped electrodes (E5-E8) is lower compared to the others.

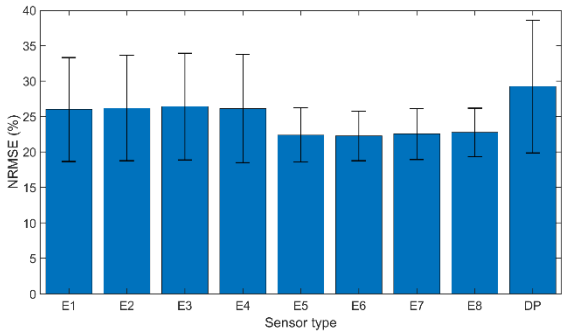

Fig. 18. NRMSE of predicted mass flow rates based on the individual sensors.

Table IV describes the name of the sensors used in each combination. The NRMSE values and standard deviations of each combination are shown in Fig. 18. The NRMSE does not improve much after the combination (vi), therefore the combination (vi) is selected for the processing in subsequent sections.

TABLE IV
COMBINATIONS OF SENSORS APPLIED TO SVM MODEL AND THEIR NRMSE

Combination label	Sensor combination	NRMSE (%)
i	E5	22.29
ii	E5, E6	21.63
iii	E5, E6, E7	20.85
iv	E5, E6, E7, E1	18.56
v	E5, E6, E7, E1, E2	17.10
vi	E5, E6, E7, E1, E2, DP	16.07
vii	E5, E6, E7, E1, E2, DP, E3	16.05
viii	E5, E6, E7, E1, E2, DP, E3, E4	16.05
ix	E5, E6, E7, E1, E2, DP, E3, E4, E8	16.04

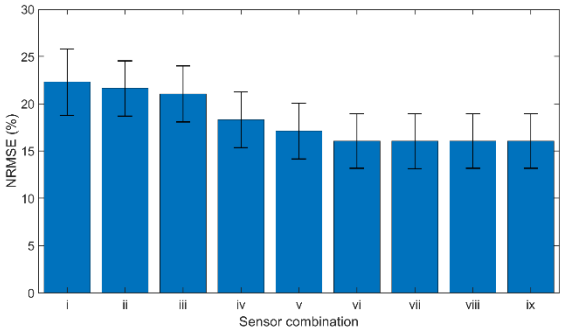

Fig. 19. NRMSE of predicted mass flow rates based on the combination of sensors.

E. Implementation and Training of Data Driven Models

As discussed in Section III-B, characteristics of the sensor signals depend on the mass flow rate as well as the velocity of solids. In order to obtain the mass flow rate of solids under different air velocity and solid flow conditions, data driven models including ANN, SVM and CNN are implemented.

Since the accuracy of the data driven models is highly dependent on the number of samples used to train the models, it is crucial to find the optimum value of the window size, which defines the length of the data that must be taken to extract the features to create a single sample. The ratio of the overall data length to the window size defines the number of samples that can be used for the training and the testing of the models. Therefore, with a fixed overall data length, a smaller window size will produce more number of samples. The overall data length is a product of data recording duration under one mass flow rate and velocity case (30 s), number of mass flow rates of solids (11) and the number of air velocities (9). As the flow of particles from the vibratory feeder via the test section of the pneumatic pipeline to the suction pump is often uneven, which can result in slight variations in the sensor signals, a small window size, e.g. 2 s, can result in large fluctuations in the extracted features. Depending on the robustness of the models, different window sizes can impact the accuracy of the models differently. An iterative analysis was carried out to evaluate the optimal size of the window for each of the data driven models, as listed in Table V. A window size below the minimum value can negatively influence the performance of the models. A larger window size is good for the accuracy of the models, but more data are acquired and processed. The CNN model, in this case, is ideal in terms of the window size requirement. However, in this study, the basis for making a comparison between the

three models is on the prediction accuracy and not on the window size requirement. Therefore, to have a fair comparison between the three models, a larger window size of 10 s is used in this study. However, for practical applications a window size of 1-2 s is appropriate to track significant changes in flow conditions. In this case, the CNN model is advantageous as it requires 2 s of data to yield the satisfactory predictions.

TABLE V
DATA SLICING OF ANN, SVM AND CNN

Model	Overall data length(s)	Minimum window size (s)	No. of samples
ANN	2970	10	297
SVM	2970	6	495
CNN	2970	2	1485

For the purpose of training the data driven models, a total of 113 features are selected from the available 390 (Table I) through the use of the PMI algorithm (Section II.E). Table VI summarizes these features that contain all the following two characteristics determined through the PMI value of each feature:

1) Selected features have a high degree of relevance with the target output.
2) Selected features have a low value of redundancy with each other.

The features are selected mainly because they provide substantial information amongst others to determine the mass flow rate of solids. The number of selected features is different for each category of sensors and this is mainly due to the reason that for some of the statistical features, a sensor that appears first in the array of electrostatic sensors (E1) has provided enough information. Selection of the same statistical feature for the sensor appearing at the second place in the array (E2) will yield a redundant information, for example, WL in this case. A similar trend is also seen for the feature count in the arc-shaped sensors, for example, E5a, E6a and E7a. It has to be noted that the orientation of the pipe does not affect the magnitude of the signals from sensors and hence the patterns of the signals, as shown in Section III-B and III-C. Therefore, all the selected features will remain same regardless of the pipe orientation. It must be pointed out that, despite the fact that we have a certain knowledge of correlations between the sensor signals, the DP transducer output and the flow characteristics, it is not straightforward to interpret the exact physical meanings of all the features. This is a common challenge when data driven modelling techniques are applied to resolve difficult measurement problems. With the development of on-going analytical modelling of gas-solids two-phase flow, engineering judgements in the application of modern machine learning techniques may have a part to play in future.

TABLE VI
FEATURES SELECTED BY PMI

Sensor	Selected features	Feature count
E1	RMS_T, σ, VAR_T, PP, SSI, WL, A_p, $\bar{C}$, RMS_{TF}, VAR_{TF}	10
E2	RMS_T, σ, VAR_T, PP, SSI, A_p, $Mean_{TF}$, VAR_{TF}	8
E5a	RMS_T, σ, VAR_T, PP, SSI, WL, A_p, $\bar{C}$, RMS_{TF}, VAR_{TF}	10
E5b	RMS_T, σ, ZC, VAR_T, PP, SSI, SSL, A_p, $\bar{C}$, RMS_{TF}	10
E5c	RMS_T, σ, PP, SSL, $\bar{C}$, RMS_{TF}	6
E5d	RMS_T, σ, VAR_T, PP, SSI, WL, A_p, $\bar{C}$, RMS_{TF}, VAR_{TF}	10
E6a	RMS_T, σ, VAR_T, PP, SSI, A_p, $\bar{C}$, RMS_{TF}	8
E6b	RMS_T, σ, VAR_T, PP, SSI, SSL, A_p, RMS_{TF}	8
E6c	RMS_T, σ, A_p, $\bar{C}$, RMS_{TF}	5
E6d	RMS_T, σ, VAR_T, WL, SSL, A_p, $\bar{C}$, RMS_{TF}, VAR_{TF}	9
E7a	RMS_T, σ, VAR_T, SSI, WL, RMS_{TF}, VAR_{TF}	7
E7b	RMS_T, σ, VAR_T, SSI, A_p, RMS_{TF}, VAR_{TF}	7
E7c	RMS_T, σ	2
E7d	RMS_T, σ, VAR_T, A_p, $\bar{C}$, RMS_{TF}, VAR_{TF}	7
DP	RMS_T, $\bar{x}$, σ, VAR_T, SSI, A_p	6

The data driven models are reinitialized and retrained several times with different parameters to develop the optimized structure. The optimized internal parameters of the ANN and the SVM models are listed in Table VII. For the development of the ANN model, sigmoid activation function provides a more generic solution for the non-linear input data to map it into mass flow rate of solids. The tuning of weight values of the ANN model is undertaken with backpropagation method owing to the reason that it is simplest in structure and takes less time to converge. However, in the case of the SVM model, radial basis function (RBF) is one of the most suitable kernel functions for the non-linear input data. RBF is preferred when there is no prior knowledge available about the input data. Based on the nature of the sensor data, RBF has appropriately transformed the input data into another feature space where the data is suitably mapped into the correct mass flow rates of solids. SMO is used as a solver to solve the quadratic programming problem for the SVM model. SMO works as an iterative algorithm that breaks down the whole optimization problem into small sub-problems which can be solved analytically. A separate cost function works in conjunction with SMO to evaluate the solution. The choice for the rest of the parameters of the ANN and SVM models is based on the best trade-off between the training time of the models and the level of prediction accuracy.

The layers and parameters of the CNN model are designed and selected through trial and error by keeping in mind the factors mentioned in Section II-F. Development of the CNN model started by keeping the lower number of convolutional layers with a smaller sized convolution window. The number of layers is then increased in each iteration until the accuracy reached saturation. The optimized CNN model, with the parameters listed in Table VIII, is comprised of multiple layers that include Convolutional Layer (CL), Batch Normalization Layer (BNL), Max Pooling Layer (MPL), Rectified Linear Unit (ReLu), SoftMax Layer, Dropout Layer, and Fully Connected Layer. In the first layer, 20,000 post-processed samples extracted from each of the 15 sensors in combination (combination vi in Table IV) are stored in 15 different rows constituting an image matrix of dimension 15×20000. In the subsequent layers, this image data pass through 12 convolutional layers with different sized convolution windows and the stride values to extract the information. The convolution layer is the core of the CNN model to extract the meaningful information. The dimension of the input data is substantially

high, therefore a set of multiple convolution layers with a high range of window sizes is applied to gather most of the useful information from the input data. An optimized number of convolution layers is selected by trading off between prediction accuracy and the processing time by iteratively adding more and more layers. An MPL with a standard window size is only used in the 2nd layer to reduce the dimension of the data to a reasonable level. MPL is chosen over average pooling layer (AVL) due to its supremacy in prediction accuracy. However, BNL and ReLu are the parts of each hidden layer purpose of which is to standardize the input for each mini batch and to keep the values in positive range, respectively.

Apart from process of designing the layer, there are some parameters which need to be selected prior to training of the model, as summarized in Table IX. Batch size in the training process defines the number of images that can be processed by all the layers of CNN in one time. As the dimension of input data is high, therefore a smaller batch size is chosen to process the data appropriately. In order to bring the level of loss function below 5%, all the training data is repeated in 30 epochs. The model parameters are updated in each iteration based on the parameters of the previous iteration with a momentum. Setting the momentum to zero or one defines no contribution or maximal contribution from the previous iteration, respectively. A constructive difference is observed in the performance by keeping the momentum between 0.8 and 1. The value of the initial learning rate lies between 0 and 1. A very small or exceedingly large learning rate can slow down the process or cause the learning to stop prematurely. The CNN model narrows down the volume of information in each epoch and requires a smaller value of learning factor. Therefore, a learning factor is chosen initially to be 0.05 and then decreased in each epoch by a drop factor of 0.002. Lastly, the training process terminates if the number of times the loss function keeps giving the value greater than the previous smallest loss as similar as the validation patience.

TABLE VII
PARAMETERS OF THE ANN AND SVM MODELS

Parameter	ANN	SVM
Type of model	Regression	Regression
Activation/Kernel Function	Sigmoid	RBF
No. of hidden layers	1	1
No. of hidden nodes	35	25
Input dimension	114	114
Iterations Utilized	157	445
Solver	Back propagation	SMO

TABLE VIII
OPTIMIZED PARAMETERS OF THE CNN MODEL

Layer no.	Name of layer and size
1	15 X 20000 Image Input Layer
2	4 X 4 CL with stride of 4, BNL, ReLu, 4 X 4 MPL
3	4 X 4 CL with stride of 2, BNL, ReLu
4	8 X 8 CL with stride of 4, BNL, ReLu
5	16 X 16 CL with stride of 8, BNL, ReLu
6	16 X 16 CL with stride of 4, BNL, ReLu
7	32 X 32 CL with stride of 8, BNL, ReLu
8	32 X 32 CL with stride of 4, BNL, ReLu
9	32 X 32 CL with stride of 4, BNL, ReLu
10	64 X 64 CL with stride of 8, BNL, ReLu
11	64 X 64 CL with stride of 4, BNL, ReLu
12	64 X 64 CL with stride of 2, BNL, ReLu
13	128 X 128 CL with stride of 2, BNL, ReLu
14	SoftMax Layer
15	Dropout Layer
16	Fully Connected Layer
17	Regression Layer

TABLE IX
TRAINING PARAMETERS OF THE CNN MODEL

Parameter	Value
Batch size	6
Max epochs	30
Momentum	0.95
Initial learning rate	0.05
Learning rate drop factor	0.002
Validation patience	20

F. Mass Flow Rate Measurement Under Horizontal Pipe Orientation

Fig. 20 to Fig. 22 show the predicted mass flow rates of solids with the ANN, SVM and the CNN models, respectively, under horizontal pipe orientation. Results for each model are compared with the ideal straight line that shows the proximity of the predicted results to the reference mass flow rate. The models are tested for eleven different mass flow rates of solids under each of which there are nine different air velocities. The outputs of the data driven models are based on the random values of the weights and the biases in the structure, therefore the predicted mass flow rates are randomly distributed around the reference lines.

The error in the predicted mass flow rates of solids under unseen test conditions is higher than that under the seen test conditions. Fig. 23 shows the poor generalization ability of the ANN model with maximum relative error of 18%. The higher prediction error at lower mass flow rates of solids (< 7.7 g/s) is due to the extremely dilute volumetric concentration of solids. The higher air velocities (> 25.3 m/s) cause more dilute two-phase flow that yields higher error in the predictions under unseen mass flow rates. Compared to the ANN model, the SVM performs better due to its improved generalization abilities and keeps the relative error within ±13%, as shown in Fig. 24. The SVM model avoids the over-fitting of data by maintaining a balance between the prediction error at validation and the unseen dataset. The validation dataset, in this case, is a portion of seen test conditions. Therefore, the prediction error with the SVM model for unseen mass flow rates is not significantly higher than those seen mass flow rates. The CNN model performs well when there is a high volume of sensor data that can be used to formulate enough images to input the model. The relative error between the measured and the actual mass flow rates of solids remains within ±2% under all conditions except the mass flow rates 3.2 g/s and 35.8 g/s which lie out of the training data range. The cross-sectionally averaged and localized particle velocity are also applied as input features for the models. For this reason, the error in the predicted mass flow rate of solids is also dependent on the ability of the data driven models to suitably fit all the data with such complexity.

From Fig. 26 to Fig. 28, it is evident that the maximum normalized standard deviation (NSTD) of the predicted mass flow rates of solids with the trained ANN, SVM and the CNN

models remains within 14%, 8% and 5%, respectively. The comparison between the NSTD values for the three models also shows that the predictions made with the CNN are more repeatable than the ANN and SVM models.

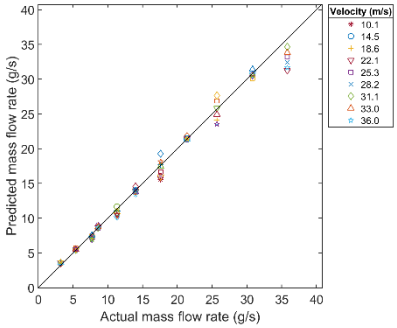

Fig. 20. Mass flow rate measurement with ANN under horizontal pipe orientation.

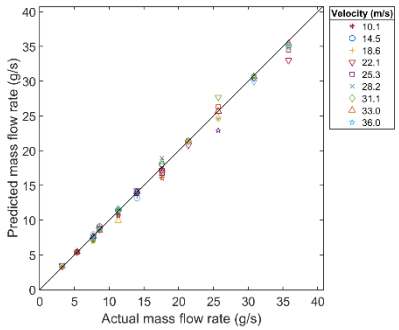

Fig. 21. Mass flow rate measurement with SVM under horizontal pipe orientation.

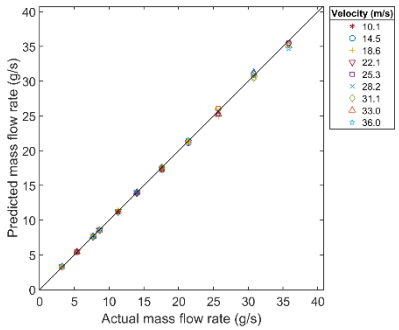

Fig. 22. Mass flow rate measurement with CNN under horizontal pipe orientation.

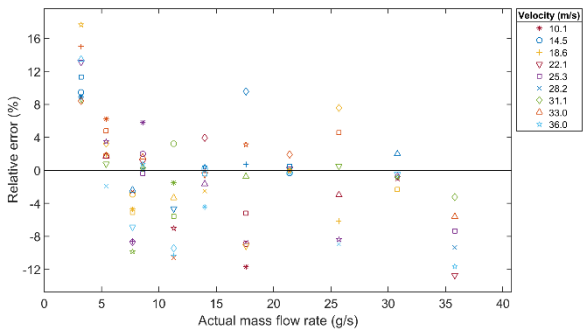

Fig. 23. Relative error with ANN under horizontal pipe orientation.

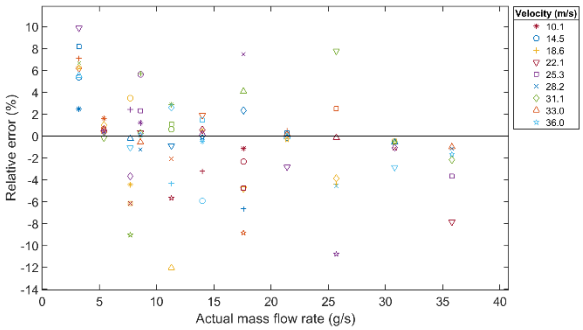

Fig. 24. Relative error with SVM under horizontal pipe orientation.

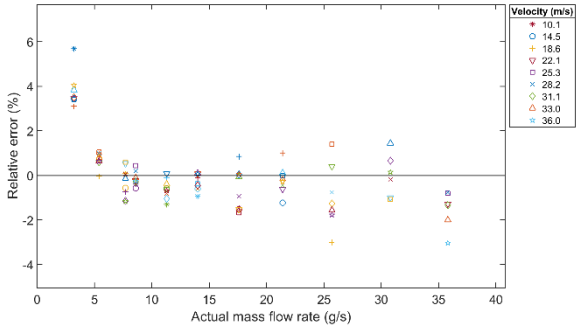

Fig. 25. Relative error with CNN under horizontal pipe orientation.

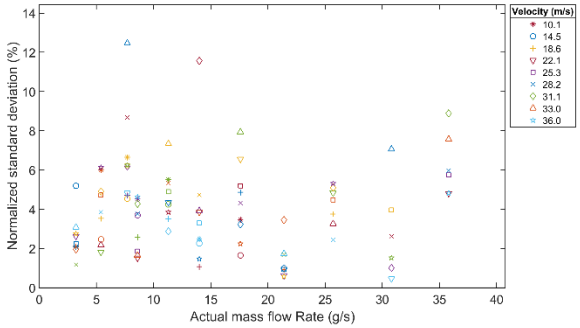

Fig. 26. Normalized SD with ANN under horizontal pipe orientation.

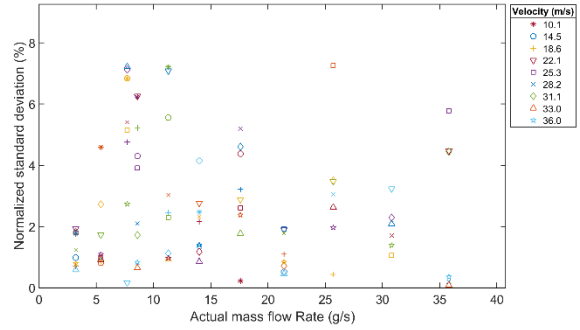

Fig. 27. Normalized SD with SVM under horizontal pipe orientation.

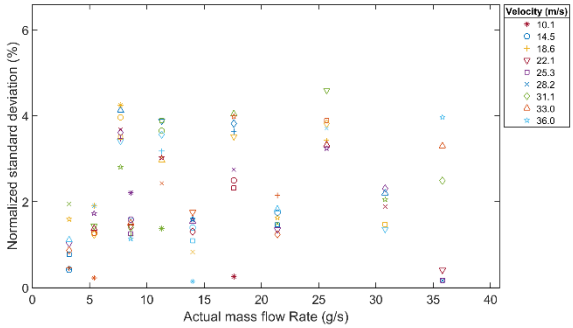

Fig. 28. Normalized SD with CNN under horizontal pipe orientation.

G. Mass Flow Rate Measurement Under Vertical Pipe Orientation

Fig. 29 to Fig. 31 plot the predicted mass flow rates of solids with the three models under vertical pipe orientation. For all the models, the predicted mass flow rates under higher velocities yield higher relative errors due to loss of solids energy after hitting with the bend of the pipeline, as can be seen in Fig. 32 to Fig. 34. The data driven models are trained and tested with a different dataset under vertical pipe orientation. Therefore, the relative errors in predictions made with the ANN, SVM and the CNN models are similar to those under horizontal pipe orientation. In the vertical pipe orientation, the ANN, SVM and the CNN model has predicted the mass flow rate of solids with relative error within ±18%, ±14%, ±8%, respectively. However, compared to those under horizontal pipe orientation, mass flow rate measurements under vertical pipe orientation are more repeatable (Fig. 35 to Fig. 37) due to the fact that, after hitting the bend of the pipeline, solids start moving downwards more consistently in the vertical pipeline. The mass flow rates predicted with ANN, SVM and the CNN model are repeatable with maximum NSTD of 13%, 8% and 5%, respectively.

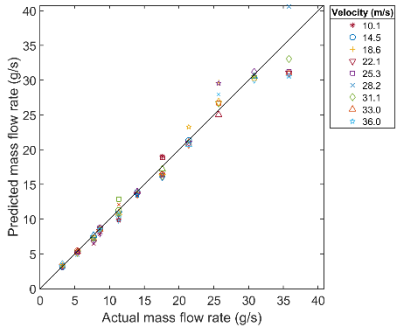

Fig. 29. Mass flow rate measurement with ANN under vertical pipe orientation.

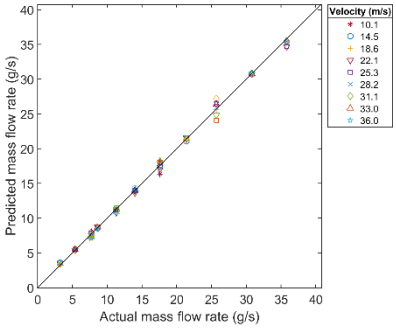

Fig. 30. Mass flow rate measurement with SVM under vertical pipe orientation.

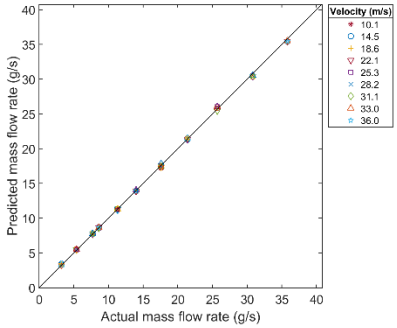

Fig. 31. Mass flow rate measurement with CNN under vertical pipe orientation.

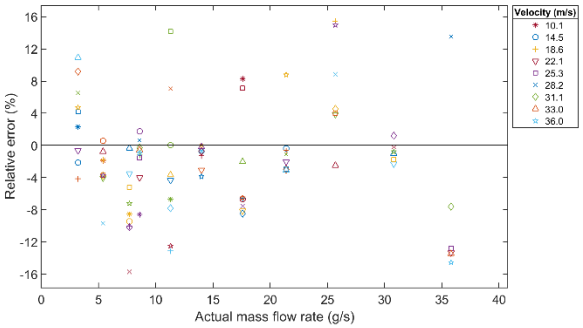

Fig. 32. Relative error with ANN under vertical pipe orientation.

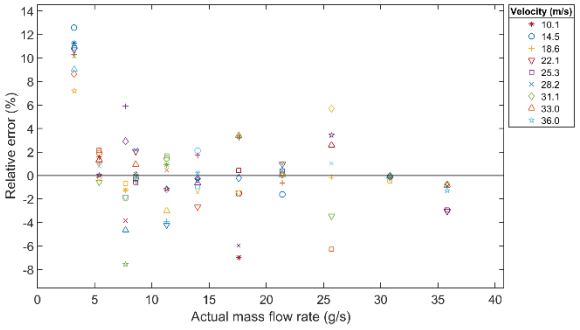

Fig. 33. Relative error with SVM under vertical pipe orientation.

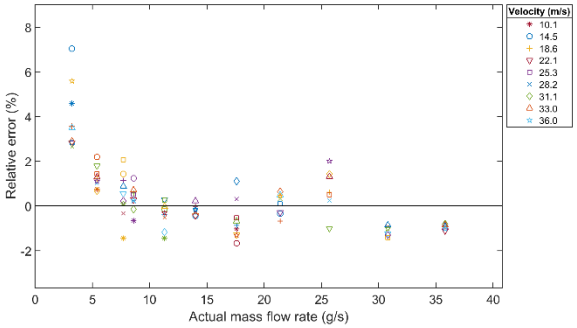

Fig. 34. Relative error with CNN under vertical pipe orientation.

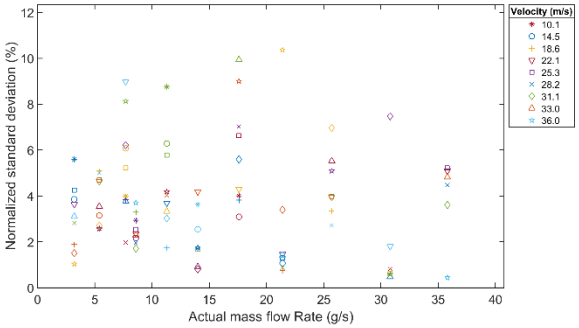

Fig. 35. Normalized SD with ANN under vertical pipe orientation.

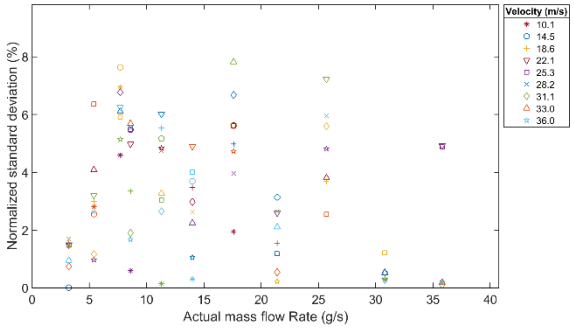

Fig. 36. Normalized SD with SVM under vertical pipe orientation.

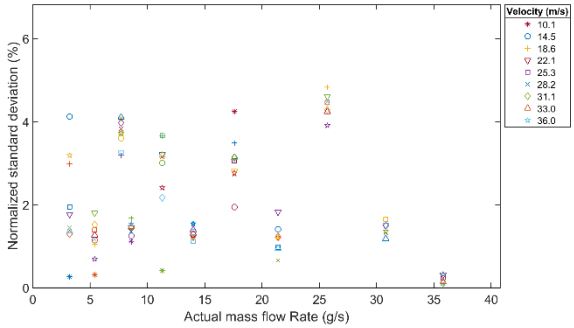

Fig. 37. Normalized SD with CNN under vertical pipe orientation.

H. Comparison of Data Driven Models

A comparison is made between the ANN, SVM and the CNN models in terms of maximum relative error and NSTD under all the seen and unseen test conditions. Table X summarizes the performance comparison between the three models. The structure of the ANN model is based on the very basic idea of a neural network where the weights and the biases are randomly initialized and tuned, which is not a suitable method to establish the relationship between the characteristics of sensor outputs and the intended measurand. For this very reason, the ANN model has not performed well for both seen and unseen conditions. However, the SVM model has generalized the data comparatively better than the ANN model because it works on the principle of transforming the data into a multi-dimensional feature space with an increasing degree of the polynomial using the kernel function to best fit the data. Furthermore, the mass flow rate measurement via the SVM model has lower NSTD values, demonstrating a better repeatability of the models. This outcome is in agreement with the earlier research on gas-liquid two phase flow measurement through SVM modelling [25] [29]. However, in comparison with both ANN and SVM models, the CNN model produces consistently more accurate and more repeatable results. This outcome is believed to be due to the fact that the CNN is capable of extracting the high-level information from the complex image data through multiple convolutional layers in an incremental method.

The maximum error and NSTD for all the models under seen test conditions are both lower than those under unseen test conditions because the models are trained with similar mass flow rates as the seen test conditions. The consistence in the solids movement in vertical pipe orientation increases after the solids hit with the bend of the pipeline. Therefore, compared to horizontal pipe orientation, the maximum error and NSTD for the seen test conditions are smaller than those in vertical pipe orientation. However, for unseen test conditions, the maximum error and NSTD remains in close agreement for both orientations.

The models are trained with different air velocities and mass flow rates of solids, therefore the generalization capability of the models has made them robust enough to predict the mass flow rate of solids under unseen test conditions. For the purpose of exploring the potential and applicability of data driven models for mass flow rate measurement of solids under different air velocities, all the other physical parameters such as pipe orientation and environmental conditions are kept constant. However, the data driven models can also be generalized for different pipe orientations and environmental conditions, provided they are trained with the data under the correct wide range of pipe orientations, ambient temperatures and relative humidity under which the sensors are to be installed for practical applications [16, 22].

It should be noted that the actual conditions in engineering can be very different from the laboratory conditions, so the models trained in a laboratory may not perform well in practical applications. In order to make the models work well in the real world, it is imperative to collect sufficient and representative datasets under actual operational conditions on the plant where the models to be deployed. The models that have been previously developed under laboratory conditions will need to be re-trained for the intended industrial application, though the overall methodology (model structure, selected features etc.) and the whole measurement system (sensors, data acquisition unit, computing unit etc.) remain the same. Moreover, an in-situ training functionality should be incorporated so that the online

training of the developed models can be updated regularly to enhance the performance of the models in the field. The main advantage of the proposed technique is that it can be applied on an industrial process plant that requires the measurement of mass flow rate of solids, provided that the datasets are collected under the actual plant conditions and are representative of the range of the conditions of the process plant. There are little changes to the hardware of the measurement system.

TABLE X
COMPARISON BETWEEN THE ANN, SVM AND CNN MODELS

		Seen test conditions			Unseen test conditions		
		ANN	**SVM**	**CNN**	**ANN**	**SVM**	**CNN**
Max. Error (%)	**Horizontal**	13.52	5.92	1.65	17.14	12.38	5.87
	Vertical	6.83	3.16	2.26	17.95	13.74	7.14
Max NSTD (%)	**Horizontal**	9.78	6.32	2.45	14.05	7.64	4.76
	Vertical	7.73	5.68	1.92	12.52	7.89	5.07

IV. CONCLUSIONS

In this study, a multi-modal sensing system, including an array of ring-shaped, four arrays of arc-shaped electrostatic sensors and a DP transducer, has been proposed for the measurement of mass flow rate of solids through data driven modelling. The results presented have suggested that, for all the seen and unseen test conditions, the CNN model has outperformed the ANN and the SVM models with a relative error within ±8% while the normalized standard deviation within 5% in both horizontal and vertical pipe orientations. The ANN and the SVM models have yielded relative errors of ±18% and ±14%, respectively, with normalized standard deviations of 14% and 8%, respectively. The direct relationship between the signal from DP transducer, particle velocity and mass flow rate of solids has constructively enhanced the performance of the models. The performance of the SVM model remains same for all the individually used electrostatic sensors for the same shaped electrodes. However, the SVM model does not perform well when trained with the combination of several electrostatic sensors from the same type of electrodes due to over-fitting problem of the model. It should be stressed that not all the sensors can provide the same number of statistical features that are useful for the data driven models. Some statistical features are useful while the others are regarded as redundant based on the partial mutual information algorithm. Compared to the ANN and SVM models, the CNN model requires a smaller window size to extract the complete information from the sensor data to produce one prediction.

Future work of this research will include evaluating the performance of the data driven models under varying ambient temperature, relative humidity and particle type as well as on full process plant conditions such as coal fired power stations.

REFERENCES

[1] D. Mills, *A review of pneumatic conveying systems. In Pneumatic Conveying Design Guide*, 3rd ed. Chatswood, NSW, Australia: Elsevier, 2016.

[2] Y. Yan, Y. Hu, L. Wang, X. Qian, W. Zhang, K. Reda, J. Wu, and G. Zheng, "Electrostatic sensors - their principles and applications," *Measurement*, vol. 169, p. 108506, Feb. 2021.

[3] R. Abdul Rahim, L. Leong, K. Chan, M. Rahiman, and J. Pang, "Real time mass flow rate measurement using multiple fan beam optical tomography," *ISA Transactions*, vol. 47, no. 1, pp. 3–14, 2008.

[4] N. O. Mahony, T. Murphy, K. Panduru, D. Riordan, and J. Walsh, "Acoustic and optical sensing configurations for bulk solids mass flow measurements," in *2016 10th International Conference on Sensing Technology (ICST)*, Nanjing, China, Nov. 2016, pp. 1–6.

[5] N. A. Zulkiflli, S. Ibrahim, M. H. F. Rahiman, J. Pusppanathan, R. A. Rahim, K. S. Tee, F. A. Phang, N. D. Nawi, and N. M. N. Ayob, "Ultrasound tomography hardware system for multiphase flow imaging," in *2019 IEEE International Conference on Signal and Image Processing Applications (ICSIPA)*, Kuala Lumpur, Malaysia, Sep. 2019, pp. 264–268.

[6] X. Wang, Y. Hu, H. Hu, and L. Li, "Evaluation of the performance of capacitance sensor for concentration measurement of gas/solid particles flow by coupled fields," *IEEE Sensors Journal*, vol. 17, no. 12, pp. 3754–3764, June 2017.

[7] A. Bilgic, J. Kunze, V. Stegemann, J. Hogendoorn, and M. Zoeteweij, "Multiphase flow metering with nuclear magnetic resonance spectroscopy," in *AMA Conferences*, Nurnberg, Germany, May 2015, pp. 292–297.

[8] J. Li, F. Fu, S. Li, C. Xu, and S. Wang, "Velocity characterization of dense phase pneumatically conveyed solid particles in horizontal pipeline through an integrated electrostatic sensor," *International Journal of Multiphase Flow*, vol. 76, pp. 198–211, Nov. 2015.

[9] Y. Zheng and Q. Liu, "Review of techniques for the mass flow rate measurement of pneumatically conveyed solids," *Measurement*, vol. 44, no. 4, pp. 589–604, May 2011.

[10] Y. Hu, Y. Yan, X. Qian, and W. Zhang, "A comparative study of induced and transferred charges for mass flow rate measurement of pneumatically conveyed particles," *Powder Technology*, vol. 356, pp. 715–725, Nov. 2019.

[11] X. Qian, Y. Yan, X. Huang, and Y. Hu, "Measurement of the mass flow and velocity distributions of pulverized fuel in primary air pipes using electrostatic sensing techniques," *IEEE Transactions on Instrumentation and Measurement*, vol. 66, no. 5, pp. 944–952, May 2017.

[12] X. Qian, X. Huang, H. Yonghui, and Y. Yan, "Pulverized coal flow metering on a full-scale power plant using electrostatic sensor arrays," *Flow Measurement and Instrumentation*, vol. 40, pp. 185 – 191, 2014.

[13] J. B. Gajewski, "Electrostatic nonintrusive method for measuring the electric charge, mass flow rate, and velocity of particulates in the two-phase gas-solid pipe flows - its only or as many as 50 years of historical evolution," *IEEE Transactions on Industry Applications*, vol. 44, no. 5, pp. 1418–1430, Sep. 2008.

[14] X. Qian and Y. Yan, "Flow measurement of biomass and blended biomass fuels in pneumatic conveying pipelines using electrostatic sensor-arrays," *IEEE Transactions on Instrumentation and Measurement*, vol. 61, no. 5, pp. 1343–1352, May 2012.

[15] Y. Yan, L. Wang, T. Wang, X. Wang, Y. Hu, and Q. Duan, "Application of soft computing techniques to multiphase flow measurement: A review," *Flow Measurement and Instrumentation*, vol. 60, pp. 30–43, Apr. 2018.

[16] F. Abbas, Y. Yan, and L. Wang, "Mass flow measurement of pneumatically conveyed solids through multi-modal sensing and machine learning," in *2020 IEEE International Instrumentation and Measurement Technology Conference (I2MTC)*, Dubrovnik, Croatia, May 2020.

[17] K. T. Aminu, D. McGlinchey, and A. Cowell, "Acoustic signal processing with robust machine learning algorithm for improved monitoring of particulate solid materials in a gas flowline," *Flow Measurement and Instrumentation*, vol. 65, pp. 33 – 44, Mar. 2019.

[18] X. Wang, H. Hu, and A. Zhang, "Concentration measurement of three-phase flow based on multi-sensor data fusion using adaptive fuzzy inference system," *Flow Measurement and Instrumentation*, vol. 39, pp. 1–8, Jun. 2014.

[19] P. Zhang, Y. Yang, Z. Huang, J. Sun, Z. Liao, J. Wang, and Y. Yang, "Machine learning assisted measurement of solid mass flow rate in horizontal pneumatic conveying by acoustic emission detection," *Chemical Engineering Science*, vol. 229, p. 116083, Jan. 2021.

[20] Y. Yan, B. Byrne, S. Woodhead, and J. Coulthard, "Velocity measurement of pneumatically conveyed solids using electrodynamic sensors," *Measurement Science and Technology*, vol. 6, no. 5, pp. 515–537, May 1995.

[21] Y. Yan, L. Xu, and P. Lee, "Mass flow measurement of fine particles in a pneumatic suspension using electrostatic sensing and neural network

techniques," *IEEE Transactions on Instrumentation and Measurement*, vol. 55, no. 6, pp. 2330–2334, Dec. 2006.
[22] F. Abbas, L. Wang, and Y. Yan, "Mass flow rate measurement of solids in a pneumatic conveying pipeline in different orientations," *Measurement: Sensors*, vol. 10-12, p. 100021, Nov. 2020.
[23] A. Darudi, S. Rezaeifar, and Mohammd Hossein Javidi Dasht Bayaz, "Partial mutual information based algorithm for input variable selection for time series forecasting," in *2013 13th International Conference on Environment and Electrical Engineering (EEEIC)*, Wroclaw, Poland, Nov. 2013, pp. 313–318.
[24] L. Wang, Y. Yan, X. Wang, and T. Wang, "Input variable selection for data-driven models of Coriolis flowmeters for two-phase flow measurement," *Measurement Science and Technology*, vol. 28, no. 3, p. 035305, feb 2017.
[25] L. Wang, J. Liu, Y. Yan, X. Wang, and T. Wang, "Gas-liquid two-phase flow measurement using Coriolis flowmeters incorporating artificial neural network, support vector machine and genetic programming algorithms," *IEEE Transactions on Instrumentation and Measurement*, vol. 66, no. 5, pp. 852–868, May 2017.
[26] G. J. Bowden, G. C. Dandy, and H. R. Maier, "Input determination for neural network models in water resources applications," *Journal of Hydrology*, vol. 301, no. 1, pp. 75 – 92, Jan. 2005.
[27] C. Nwankpa, W. Ijomah, A. Gachagan, and S. Marshall, "Activation functions: Comparison of trends in practice and research for deep learning," in *2nd International Conference on Computational Sciences and Technologies*, Jamshoro, Pakistan, Dec. 2020, pp. 124–133.
[28] A. Khan, A. Sohail, U. Zahoora, and A. S. Qureshi, "A survey of the recent architectures of deep convolutional neural networks," *Artificial Intelligence Review*, vol. 53, no. 1, pp. 5455–5516, Apr. 2020.
[29] L. Wang, Y. Yan, X. Wang, T. Wang, Q. Duan, and W. Zhang, "Mass flow measurement of gas-liquid two-phase co2 in ccs transportation pipelines using Coriolis flowmeters," *International Journal of Greenhouse Gas Control*, vol. 68, pp. 269–275, Jan. 2018.